Crystallinity-modulated Co₂₋ₓVₓO₄ Nanoplates for Efficient Electrochemical Water Oxidation

Chaoran Jiang,[1‡] Ji Yang,[2,3‡] Xiaoyu Han,[4‡] Haifeng Qi,[2] Min Su,[3] Deqiang Zhao,[1] Leilei Kang,[2] Xiaoyan Liu,[2] Jianfeng Ye,[1] Jianfeng Li,[3] Zheng-Xiao Guo,[5,6] Nikolas Kaltsoyannis,[4] Aiqin Wang,[2*] and Junwang Tang[1*]

1. Department of Chemical Engineering, University College London, Torrington Place, London, WC1E 7JE, UK.

2. State Key Laboratory of Catalysis, Dalian Institute of Chemical Physics, Chinese Academy of Sciences, Dalian, 116023, P.R. China.

3. State Key Laboratory for Physical Chemistry of Solid Surfaces, iChEM, and College of Chemistry and Chemical Engineering, Xiamen University, Xiamen, 361005, P.R. China.

4. Department of Chemistry, University of Manchester, Oxford Road, Manchester, M13 9PL, UK.

5. Department of Chemistry, The University of Hong Kong, Pokfulam Road, Hong Kong, 999077, P.R. China

6. HKU Zhejiang Institute of Research and Innovation, Hangzhou, 311300, P.R. China.

Supporting Information Placeholder

ABSTRACT: Cost-efficient and durable oxygen evolution catalysts are in great demand, which are dominated not only by the component of the electrocatalysts but also by their molecular structure and crystallinity. Herein, we developed an efficient cobalt-vanadium spinel-type electrocatalyst with an extremely high concentration of Co^{3+} ions by tuning the balanced vanadium ions' concentration in a crystallinity-modulated $Co_{2-x}V_xO_4$ nanoplates. This resulted in the lowest overpotential of 240 mV at 10 mA/cm², a smallest Tafel slope of 45 mV dec⁻¹ and a current density of 100 mA/cm² at an overpotential of 280 mV for water oxidation, which is remarkably 20 times better than that of the benchmark RuO_2 catalyst, together with excellent stability. Such excellent performance is due to the very high Co^{3+}/Co^{2+} ratio of 2.84 achieved in-situ in the low crystallinity $Co_{2-x}V_xO_4$ (LC-$Co_{2-x}V_xO_4$) sample, which is 40 % higher than the widely reported Co_3O_4 as evidenced by both operando XANES and in-situ XPS. These findings stimulate the opportunities to explore $Co_{2-x}V_xO_4$ as a class of nonprecious meal-based efficient OER electrocatalysts.

KEYWORDS: electrocatalysts, water oxidation, cobalt-vanadium cluster, crystallinity, nanoplates

Electrochemical water splitting offers a feasible way to store sustainable energy in the form of hydrogen.[1] However, the oxidative half reaction of water splitting, oxygen evolution reaction (OER) is kinetically extremely sluggish due to the proton-coupled four electron transfer process, which limits the overall efficiency of water splitting.[2-4] RuO_2 and IrO_2 are considered as the benchmark OER catalysts with low overpotentials, typically ca. 300 mV at the current density of 10 mA/cm², whereas the high cost and/or instability of these catalysts limit their large-scale applications.[5,6] In the last few years, substantial effort has been devoted to exploring cost-effective, robust and highly efficient OER catalysts.[3,7,8] With comparable activities to precious metal-based catalysts, earth-abundant cobalt-based oxides (perovskites or spinels), hydroxides and layered double hydroxides (LDHs) have become increasingly attractive.[9-11] For example, thin-film of perovskite-based strontium cobaltite ($SrCoO_x$) with optimised oxygen vacancy concentration displayed catalytic performance of OER commensurate with noble-metal electrodes such as IrO_2.[12] Low-temperature prepared spinel-type lithium cobalt oxide (LT-$LiCoO_2$) was reported as an efficient OER catalyst with slightly higher activity than IrO_2.[13] CoOOH nanosheets with partial iron substitution ($Co_{0.67}Fe_{0.33}OOH$) exhibited about 24 mV lower overpotential at 10 mA/cm² compared to IrO_2.[14]

The importance of Co^{3+} for active OER was recognised for cobalt-based materials such as Co_3O_4,[15] $CoSe$,[16] and $Co_3(PO_4)_2$.[17] Co^{3+} was prevalently believed to be able to enhance the electrophilicity of materials and facilitate the formation of *OOH intermediates and

thus O_2.[18] On the other hand, there is an ongoing contradictory factor on the importance of structural disorder or degree of crystallinity on the catalytic activity of cobalt-based oxides and hydroxides, which is generally related to the defects or vacancies, and the spin states or electronic configuration. In particular, Yamauchi et al. reported the superior catalytic activity of OER and stability of mesoporous cobalt phosphate with crystallised walls, which offered a large number of active sites and better mass transportation at the electrolyte-catalyst interface.[19] Thus, cobalt-based oxides with high crystallinity have been regarded as more stable than those amorphous ones during OER process due to the strong crystal lattice constraint. On the other hand, recent work widely reported that the electrocatalysts at amorphous states exhibited better activity than those of crystalline states.[20,21] It has been further demonstrated that the activity of the cobalt-based oxides could be dramatically increased by introducing oxygen vacancies in high-crystallinity cobalt oxides. For example, Liu et al. found that lattice distortion of spinel Co_3O_4 led to the massive high-spin Co^{3+} in octahedron sites, accompanied by rich oxygen vacancies, which would facilitate the OER activity by significantly enhancing the overlap of the e_g orbital of cobalt with the oxygen adsorbates.[22] However, Shi et al. found that largely increasing oxygen vacancies in the double perovskite $PrBaCo_2O_{6-\delta}$ would lead to cobalt ions spin state transition from high-spin to low-spin, resulting in significant reduction in the intrinsic OER activity.[23] Xie et al. further proved that the optimal spin state of cobalt or e_g electron filling in perovskite $LaCoO_3$ achieved by adjusting the degree of distortion of the CoO_6 octahedron would dramatically lower the adsorption free energy of oxygen intermediates, which resulted in 6 times higher mass activity than the counterpart.[24] Moreover, Zou et al. found that well crystallised cobalt-based OER electrocatalyst performed water oxidation on the crystal surface with no ions penetrating the bulk, leading to low catalytic efficiency.[20] Therefore, they tuned crystallinity of spinel $CoGa_2O_4$ and found that low-crystallinity $CoGa_2O_4$ could achieve a stable and efficient bulk electrocatalysis.[20] Du et al. further demonstrated the spin state of cobalt nickel oxide could be remarkably affected by the lattice distortion, which was inversely related to the crystallinity.[25]

According to these very informative studies, one can conclude that not only Co^{3+} concentration but also the degree of disorder or the crystallinity affects the electrocatalytic activity of cobalt-based electrocatalysts. In this work, we targeted to control the crystallinity and more importantly dramatically improve the concentration of Co^{3+} by synthesising a class of cobalt-vanadium (Co-V) bimetallic electrocatalysts via a one-step coprecipitation method. The components and crystallinity of Co-V bimetallic electrocatalysts could be readily controlled by varying the vanadium ions concentration introduced. The relatively low-crystallinity $Co_{2-x}V_xO_4$ showed both stable and efficient water oxidation, resulting in a very low overpotential of 240 mV at 10 mA/cm² and excellent stability, much better than the commercial benchmark catalyst RuO_2 in both overpotential and stability. The reason behind this novel property has been proved by operando and in-situ spectroscopies due to the controlled CoO_{6-x} distortion with rich Co^{3+}-O-V^{4+} catalytic active sites, which not only contribute to the high concentration of Co^{3+} but also stabilize such Co^{3+} states. This approach is believed to be applied to other types of cobalt-based oxides or hydroxides and open new opportunities to achieve efficient electrocatalysts.

The Co-V bimetallic oxides $Co_{2-x}V_xO_4$/CoOOH composite ($Co_{2-x}V_xO_4$/CoOOH, where 0 < x < 2), low-crystallinity $Co_{2-x}V_xO_4$ sample (LC-$Co_{2-x}V_xO_4$, where 0 < x < 2), amorphous $Co_{2-x}V_xO_4$ (A-$Co_{2-x}V_xO_4$, where 0 < x < 2) and counterparts (CoOOH and $V(OH)_x$) were synthesized at 50 ℃ in a water bath by dropping an alkaline solution into a solution containing cobalt chloride and/or vanadium chloride (see the methods part for details). In the following text, $Co_{2-x}V_xO_4$/CoOOH, LC-$Co_{2-x}V_xO_4$, A-$Co_{2-x}V_xO_4$ are employed as the short name for the prepared Co-V bimetallic oxides composite, low-crystallinity and amorphous $Co_{2-x}V_xO_4$ samples (0 < x < 2), respectively. The Co/V ratio in the synthesis can affect the component and crystallinity as shown in the X-ray diffraction (XRD) patterns of the as-prepared materials (**Figure 1a**). Without vanadium incorporation, the diffraction peaks can be indexed to highly crystallised CoOOH with pure heterogenite phase. While introducing some vanadium species (Co/V molar ratio = 3/1), a composite material of $Co_{2-x}V_xO_4$ /CoOOH is obtained due to the over-dose of cobalt feedstock. Further increasing the vanadium content to a proper concentration, i.e. 50 % (Co/V = 1/1), a pure spinel Co_2VO_4-like material with relatively low crystallinity (denoted as LC-$Co_{2-x}V_xO_4$) is obtained. The crystallinity is further reduced when the vanadium content is up to 75 % (Co/V = 1/3), resulting in an amorphous structure (denoted as A-$Co_{2-x}V_xO_4$). One can conclude that the vanadium doping concentration could readily modulate the structure and crystallinity. Further annealing treatment of LC-$Co_{2-x}V_xO_4$ at 300℃ in the air for 2 h dramatically increased the crystallinity, resulting in highly crystallised spinel Co_2VO_4-like material (denoted as HC-$Co_{2-x}V_xO_4$). The chemical environment

of the as-prepared catalysts was further investigated by Raman spectroscopy (**Figure 1b**). The CoOOH displays a single intense band at 503 cm^{-1}, which can be assigned to the E_g vibration mode of CoOOH.[26-28] V(OH)$_x$ exhibits four distinct bands located at 281, 407, 697 and 997 cm^{-1}, in agreement with the characteristic peaks of reported lepidocrocite VOOH.[29] In detail, the first two peaks at 281 and 407 cm^{-1} are assigned to the bending vibration of the V=O bonds.[30] The peak at 697 cm^{-1} is assigned to the doubly coordinated oxygen (V$_2$–O) stretching mode which results from corner-shared oxygens.[30] The relatively sharp peak at 997 cm^{-1} corresponds to the stretching mode of terminal oxygen (V=O).[31] For Co-V bimetallic oxides (Co$_{2-x}$V$_x$O$_4$/CoOOH, LC-Co$_{2-x}$V$_x$O$_4$ and A-Co$_{2-x}$V$_x$O$_4$), new additional bands are observed in the 750-900 cm^{-1} region, which can be attributed to the stretching vibrations of the VO$_4$ tetrahedron with A$_1$ symmetry.[32,33] The cobalt cations may be bonded with each oxygen atom of a VO$_4$ tetrahedral to form Co-O-V-O species, introducing some asymmetry in the VO$_4$ unit without disturbing the overall symmetry of the elementary unit cell.[34,35] Moreover, a clear shift toward higher wavenumber in the 750-900 cm^{-1} band is also observed with increasing vanadium content or in other words, decreasing the crystallinity which is very likely due to the local distortion caused by vanadium substitution in Co-V bimetallic oxides. Such feature of Raman bands shift was also observed on CoCr$_{2-x}$V$_x$O$_4$.[36] The Raman spectrum of HC-Co$_{2-x}$V$_x$O$_4$ shows a narrow peak at 805 cm^{-1} in comparison with LC-Co$_{2-x}$V$_x$O$_4$, indicating the crystallinity enhancement after annealing, as proved in XRD as well (**Figure 1a**).

The 2D nanoplate-like morphology of as-synthesized LC-Co$_{2-x}$V$_x$O$_4$ can be observed from scanning electron microscopy (SEM) and transmission electron microscopy (TEM) images (**Figure 1c and d**). The thickness of these vertical nanoplates is found to be ca. 5 nm. Notably, the Co/V ratio in the synthesis can affect the morphology of the as-prepared materials as well. As shown in Figure S1, when low content of vanadium exists in Co-V bimetallic oxides, Co$_{2-x}$V$_x$O$_4$/CoOOH composite and LC-Co$_{2-x}$V$_x$O$_4$ have similar morphology of nanoplates, but relatively thinner than CoOOH. However, the nanoplate morphology is destroyed with further increasing the vanadium content, where A-Co$_{2-x}$V$_x$O$_4$ and V(OH)$_x$ catalysts were obtained. The TEM elemental mappings of the LC-Co$_{2-x}$V$_x$O$_4$ (**Figure 1e**) indicate the elements Co, V and O are dispersed uniformly throughout the nanoplates. In addition, the XPS survey spectrum of LC-Co$_{2-x}$V$_x$O$_4$ shows a Co/V molar ratio of 1.7 on the surface, close to the results indicated by EDX (1.8) (**Figure S2**).

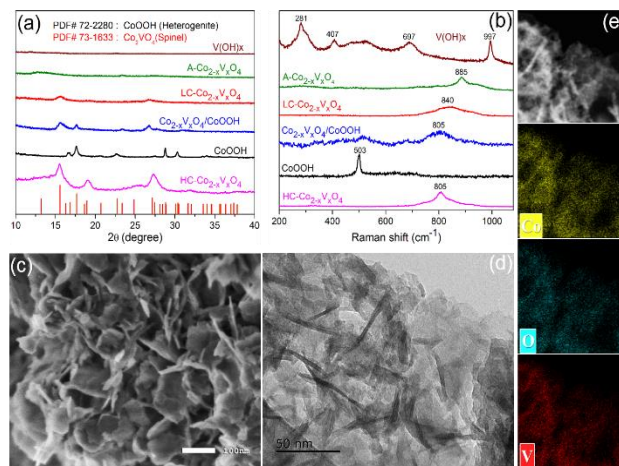**Figure 1.** (a) XRD patterns and (b) Raman spectra of CoOOH, Co$_{2-x}$V$_x$O$_4$/CoOOH composite, LC-Co$_{2-x}$V$_x$O$_4$, A-Co$_{2-x}$V$_x$O$_4$, V(OH)$_x$ and HC-Co$_{2-x}$V$_x$O$_4$. (c) SEM and (d) TEM images of LC-Co$_{2-x}$V$_x$O$_4$. (e) STEM image of LC- Co$_{2-x}$V$_x$O$_4$ and the corresponding elemental mapping for Co, O and V.

Figure 2 compares the catalytic performance of Co-V bimetallic oxides with the counterparts CoOOH, V(OH)$_x$ and commercial RuO$_2$ for the OER. As displayed in Figure 2a, the widely used commercial RuO$_2$ requires an overpotential of 300 mV to reach the 10 mA/cm^2 current, consistent with the reported value.[5,6] The reference sample CoOOH is a bit less active, resulting into an overpotential of 360 mV to obtain the 10 mA/cm^2 current, which is also consistent with previous studies,[37,38] while the V(OH)$_x$ exhibits negligible electrocatalytic activity for OER. After incorporating vanadium into the cobalt-based catalysts, the overpotentials (η@10 mA/cm^2) are significantly decreased to 280, 240 and 310 mV for Co$_{2-x}$V$_x$O$_4$/CoOOH composite, LC-Co$_{2-x}$V$_x$O$_4$ and A-Co$_{2-x}$V$_x$O$_4$, respectively, indicating vanadium doping is an efficient way to improve the electrocatalytic performance of the cobalt-based catalyst. However, further increasing the crystallinity of the LC-Co$_{2-x}$V$_x$O$_4$ unfavourably downgrades its OER activity, and thus an additional 45 mV overpotential is required to drive the 10 mA/cm^2 current for HC-Co$_{2-x}$V$_x$O$_4$. The smallest overpotential (η) of LC-Co$_{2-x}$V$_x$O$_4$ reflects its remarkable OER activity. At the current density of 10 mA/cm^2, the LC-Co$_{2-x}$V$_x$O$_4$, (η = 240 mV) shows 60 mV lower overpotential in comparison with the widely used commercial catalyst RuO$_2$ (η = 300 mV). It further exhibits a considerably low overpotential of 280 mV even at current density of 100 mA/cm^2, 70 mV lower than the benchmark commercial RuO$_2$ catalyst (η = 350 mV@100 mA/cm^2). In other words, the current density at η = 280 mV is 100 mA/cm^2 for the optimised LC-Co$_{2-x}$V$_x$O$_4$, nearly 600-folds higher than

that of CoOOH (0.175 mA/cm²), and 20 times better than that of the commercial RuO_2 (4.8 mA/cm²), respectively. The OER kinetics of the as-prepared electrocatalysts was also investigated by the corresponding Tafel slopes as depicted in Figure 2b. As expected, the LC-$Co_{2-x}V_xO_4$ exhibits the lowest Tafel slope of 45 mV dec^{-1}, which is smaller than a few state-of-the-art electrocatalysts (amorphous $CoVO_x$ with a Tafel slope of 51 mV dec^{-1} [39] and NiV-LDH with a Tafel slope of 50 mV dec^{-1}) [40] reported very recently under identical experimental conditions, indicative of the superior reaction kinetics toward OER. The overpotential of 240 mV at 10 mA/cm² of our catalyst is also much smaller compared with others e.g. 390 mV for iron-vanadium composite spheres,[41] 347 mV for amorphous $CoVO_x$,[39] 330 mV for crystallized $CoVO_x$ nanorods[35] ,318 mV for NiV-LDH ,[40] and 290 mV for CoMn-LDH electrocatalyst.[42]

The kinetics of electrode interface reactions were then studied by Electrochemical Impedance Spectroscopy (EIS) for both LC-$Co_{2-x}V_xO_4$ and HC-$Co_{2-x}V_xO_4$ (Figure 2c) to understand the effect of crystallinity. Clearly, HC-$Co_{2-x}V_xO_4$ exhibits lower charge transfer resistance (R_{ct}) than LC-$Co_{2-x}V_xO_4$, as obtained from the diameter of the semicircle in Nyquist diagrams, suggesting its superior conductivity and efficient charge transfer while the catalytic effect of LC-$Co_{2-x}V_xO_4$ is better than the former, indicating that the crystallinity is favourable to charge transfer whereas not to catalysis. To further characterise the activity stability of the LC-$Co_{2-x}V_xO_4$ catalyst, long-term durability measurement was performed as shown in Figure 2d, which shows the time-dependent overpotential required to reach 10 mA/cm² current for LC-$Co_{2-x}V_xO_4$ and the commercial RuO_2 electrocatalysts. For the LC-$Co_{2-x}V_xO_4$ electrocatalyst, the overpotential decreases in the first few hours, which is likely to be due to the activation process, in agreement with the behavior observed on others reported previously. Then the LC-$Co_{2-x}V_xO_4$ catalyst presents a very stable activity until the end of the study period of 24 h. In contrast, RuO_2 exhibits nearly 40 % overpotential increase for driving 10 mA/cm² current in 4 h measurement under identical conditions, which might be due to the oxidation of RuO_2 into a higher valence state that is more easily dissolved into the alkaline electrolyte.[5,43] Furthermore, the LSV curves before and after 24 hours OER stability test were recorded with the scan rate of 2 mV/s (Figure S3), indicating a relatively stable performance.

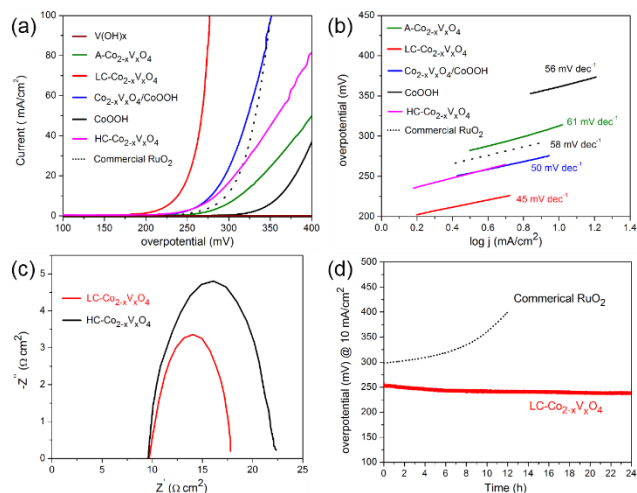**Figure 2.** (a) iR-corrected OER polarization curves and (b) Tafel slopes of CoOOH, $Co_{2-x}V_xO_4$/CoOOH composite, LC-$Co_{2-x}V_xO_4$, A-$Co_{2-x}V_xO_4$, HC-$Co_{2-x}V_xO_4$ and commercial RuO_2. (c) Electrochemical impedance spectra measured at an overpotential of 270 mV in 1 M KOH for LC-$Co_{2-x}V_xO_4$ and HC-$Co_{2-x}V_xO_4$. (d) Chronoamperometric response of LC-$Co_{2-x}V_xO_4$ and commercial RuO_2 at 10 mA/cm².

The above stability test indicates that the real active sties might be in-situ generated as the first hour is the induction time. Thus Operando synchrotron radiation X-ray absorption spectroscopy (XAS) was undertaken to give an in-depth understanding of the atomic structure of the excellent catalyst LC-$Co_{2-x}V_xO_4$. The oxidation states of Co and V can be confirmed by X-ray absorption near edge spectroscopy (XANES). As shown in Figure 3a, the Co K-edge position of fresh LC-$Co_{2-x}V_xO_4$ is very close to that of Co (OH)$_2$, indicative of the major Co oxidation state of +2 in the bulk of the fresh LC-$Co_{2-x}V_xO_4$, in part consistent with higher Co^{2+} than Co^{3+} on the surface of fresh LC-$Co_{2-x}V_xO_4$ observed later by XPS (Figure 3e). Notably, a right-shifted white line peak is observed for LC-$Co_{2-x}V_xO_4$ in comparison with Co(OH)$_2$, implying the incongruity in the coordination environment of the former.[44] Figure 3b shows that the V K-edge position of fresh LC-$Co_{2-x}V_xO_4$ is located between VO_2 and V_2O_5 while closer to the latter, suggesting the estimated V valence state of ca. +5. The pre-edge peak for the V K-edge XANES of the fresh sample is more intense than those of V_2O_5 and VO_2, indicating that vanadium species in LC-$Co_{2-x}V_xO_4$ are likely located in a VO_4 tetrahedron, different from those of VO_5 or VO_6 in V_2O_5 and VO_2, respectively.[45] The VO_4 tetrahedron can also be verified by Raman spectra as discussed in Figure 1b. In addition, the Operando XANES was employed to probe the dynamic behaviour and real active phase of LC-$Co_{2-x}V_xO_4$ during the OER process. As shown by the red dotted line in Figure 3a and 3b, after running

in-situ experiment for 5 mins at a potential of 1.5 V vs. RHE (or 270 mV of overpotential) in 1 M KOH, the absorption edge of Co in LC-Co$_{2-x}$V$_x$O$_4$ is conspicuously shifted to a higher energy position that close to that of CoOOH, which could be attributed to the oxidation of Co sites from Co^{2+} to Co^{3+}. In contrast, the V edge for LC-Co$_{2-x}$V$_x$O$_4$ slightly shifts to lower energy close to V^{4+}. The decrease of the valence state for the V species may be due to the charge transfer from cobalt to vanadium caused by strong interaction between them.[38,46] This indicates that Co^{2+} can be readily oxidised to Co^{3+} for water oxidation as observed in the Operando measurement, which is further stabilised by V^{4+}, and thus such presence of V^{4+} is favourable for highly active Co^{3+} generation that is very active during OER process.[22,35] Therefore, the improved OER performance for LC-Co$_{2-x}$V$_x$O$_4$ is owing to the high valence V^{4+}/V^{5+} ions, which could draw electrons to keep valence of neighbouring Co ions in a high-valence state for accelerating the OER process.[35,47] The higher valence cobalt species not only supply high conductivity, as proved by EIS results in Figure 2c, but also act as real active sites in OER catalysis, in agreement with previous work.[48]

The surface Co and V chemical states of LC-Co$_{2-x}$V$_x$O$_4$ were further studied by high-resolution XPS before and during OER (**Figure 3e and 3f**). Since 2p$_{3/2}$ and 2p$_{1/2}$ of cobalt and vanadium qualitatively contain the same chemical information,[49] only the higher intensity Co 2p$_{3/2}$ and V 2p$_{3/2}$ were curve-fitted in this study. As shown in Figure 3e, two peaks at 780.2 and 781.6 eV are observed for Co 2p$_{3/2}$, corresponding to Co^{3+} and Co^{2+}, respectively. The fresh sample contains more Co^{2+} than Co^{3+} while the activated sample has reverse amount, in good agreement with the Operando XANES measurement.[50,51] The ratio of Co^{3+}/Co^{2+} (2.84) for LC-Co$_{2-x}$V$_x$O$_4$ after 1 h OER exhibits an apparent increase compared to the fresh sample (1.12), implying that Co^{3+} is in-situ generated and is advantageous for activating the OER. Meanwhile, the Co^{3+}/Co^{2+} ratio keeps nearly constant after 1 h OER towards the end of the reaction (8 h), further suggesting the excellent stability of LC-Co$_{2-x}$V$_x$O$_4$, as observed from the stability measurements illustrated in Figure 2d. On the other hand, the V 2p$_{3/2}$ can be fitted into two constituent peaks corresponding to V^{4+} (516.6 eV) and V^{5+} (517.6 eV) for both fresh and activated OER samples (Figure 3f).[41] The reduced V^{5+}/V^{4+} ratio is observed for LC-Co$_{2-x}$V$_x$O$_4$ after 1 h OER, which exactly matches with the increased Co^{3+}/Co^{2+} ratio. As expected, no noticeable change of V^{5+}/V^{4+} ratio is observed after 8 h OER.

Furthermore, in Figure 3c and Table S1 of the extended X-ray absorption fine structure (EXAFS) in the R-space of LC-Co$_{2-x}$V$_x$O$_4$, the distance of the Co-O is 2.05 Å, which is longer than that of the Co-O (1.89 Å) in CoOOH. The elongation of Co-O bonds may lower the absorption energy of H$_2$O and thus improve OER performance according to the previous study.[52] Besides, it is worth highlighting that the vanadium incorporation also lowers the coordination numbers of the Co-O clusters, from 6.0 to 4.1 (Table S1), signifying that the general lattice distortion and coordination deficiency (i.e. CoO$_{6-x}$) occurs in LC-Co$_{2-x}$V$_x$O$_4$ (Figure 3c). In contrast, as shown in Figure 3d and Table S1, the LC-Co$_{2-x}$V$_x$O$_4$ exhibits higher V-O coordination number (N = 1.9) at the distance of 1.69 Å in comparison with V(OH)$_x$ (N = 1.0), which matches well with the better crystallinity than the amorphous V(OH)$_x$ (**Figure 3d**). All these spectroscopic results draw an important conclusion that vanadium incorporation leads to CoO$_{6-x}$ octahedra and VO$_4$ tetrahedra. The results from both Operando XANES and XPS confirm the oxidisation of Co and reduction of V ions during the OER for spinel Co$_2$VO$_4$-like catalyst, and the active reaction sites are Co^{3+}-O-V^{4+} species which was in-situ yielded herein.[35,45]
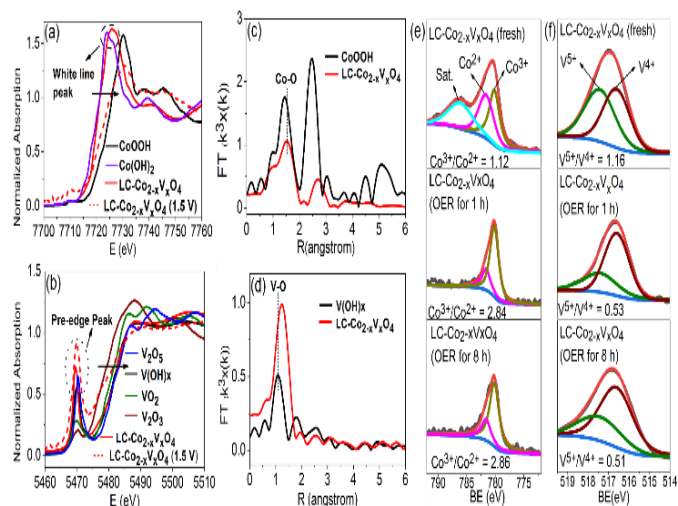

Figure 3. (a) Co K-edge and (b) V K-edge X-ray absorption near edge structure (XANES) measurements performed at the initial stage and continuous OER stage of LC- Co$_{2-x}$V$_x$O$_4$ with CoOOH, Co(OH)$_2$, V$_2$O$_3$, VO$_2$, V$_2$O$_5$ and V(OH)$_x$ as reference samples. The Operando measurements were carried out at an applied potential of 1.5 V vs RHE in 1 M KOH during the OER. (c) and (d) Fourier transformation curves of EXAFS spectra at Co and V K-edge in R space for CoOOH, V(OH)$_x$ and LC-Co$_{2-x}$V$_x$O$_4$ (without phase correction). (e) and (f) XPS high-resolution spectra of Co 2p3/2 and V 2p$_{3/2}$ of the LC-Co$_{2-x}$V$_x$O$_4$ catalyst at fresh, after 1 h OER, and after 8 h OER states, respectively.

To provide further insight into the reasons for the highly catalytic activity of OER, the electrochemical surface area (ECSA) of the studied catalysts was evaluated by measuring the double-layer capacitance (C_{dl}) in the non-faradic region in 1 M KOH because the C_{dl} is proportional to their ECSA. Figure S4 shows typical CV curves of studied catalysts (CoOOH, LC-$Co_{2-x}V_xO_4$, V(OH)x). By plotting the $\Delta J=(Ja-Jc)$ at 1.3 V vs RHE against the scan rates, the linear slope that is twice the double layer capacitance (C_{dl}) can be obtained and is normally used to represent the corresponding ECSA. The active surface area is a very important factor in water oxidation reaction, as it is well known that an increase of active surface area often benefits for the catalytic activity. The electrochemically active surface area (ECSA) of CoOOH (3.72± 0.06 mF cm-2) is nearly three times that of V(OH)x (1.24± 0.03 mF cm-2). Notably, LC-$Co_{2-x}V_xO_4$ (20.40± 0.30 mF cm-2) has a nearly 5.5-folds increasement on ECSA compared to CoOOH even they have similar nanostructure. This growth of ECSA suggests the LC-$Co_{2-x}V_xO_4$ has higher density of catalytically active sites exposed to an electrolyte to catalytic water oxidation reaction. This is a strong clue that high density of Co^{3+}-O-V^{5+} active species on LC-$Co_{2-x}V_xO_4$ are the major contributor to the large ECSA and thus highly electrochemical activity.

In order to enrich high-spin Co^{3+} to facilitate the OER, we tuned the oxidation states of the Co in the cobalt oxide by the substitution of V. It was noted that the +4 oxidation state of cobalt is unstable even it attains a half filled state, whereas the Co^{3+} shows $3d^6$ configurations where 6 electrons reside in the low energy t_{2g} level. Hence, pure Co_2O_4 does not exist in nature but heterogeneous chemical doping, e.g. by V, can be effective to stablise the modified structure. In order to verify the structure and its oxidation states, we have carried out the computational simulations. To obtain the structure of the V-doped Co_2O_4, we fully surveyed the CoO_2 structure database in Material Project.[53] By matching the three key peaks from our experimental XRD of the HC-$Co_{2-x}V_xO_4$ and the peaks of CoOOH in Figure 1(a), the symmetry group I4/m (Figure S5 (a)) was selected for the V-doped candidate. The Co:V doping ratio was set to 5:3, which is close to the 1.7 obtained from the experimental EDX results (Figure S2). The Co_3O_4 structure was obtained from the previous XRD analysis.[54] All the possible substitution geometries were studied, as shown in Figures S5 (b-f). Energetically, the structure in Figure S5(f) with the ratio of Co:V =5:3 is the most stable (the relative energy in Table S2). The Bader charge analysis in Table S3 shows that the partial charge of the Co is overall larger by 0.1 e compared with well-known +2/+3 mixed Co_3O_4. The partial charge of the Co atoms shared with 3 V linked octahedral oxygen reached 1.44 e in the most stable case. As the 2:1 ratio of +3/+2 oxidation in the Co_3O_4 shows a partial Bader charge of 1.25 , we can conclude that the +3/+2 oxidation ratio has increased to 2.24 in the simulated V doped case. The ab-initio MD results show the stability of the most stable doped structure (Movie S1). The energy of the doped system oscillated with temperature within 0.4 eV/atom, Figure S6, which indicates the structure remains stable in 400K. Hence, the V doping has stabilised the "Co_2O_4" structure to much higher average oxidation states than achievable in Co_3O_4, consistent with our experimental resutls.

The previous experimental and theoretical study established a strong evidence that structural distortion of CoO_{6-x} octahedra would enhance the electrophilicity of H_2O and facilitate the interfacial electron transfer between Co ions and adsorbed *OOH intermediates to form O_2, resulting in enhanced OER activity for CoOOH.[48] On the other hand, increasing the crystallinity of $Co_{2-x}V_xO_4$ to form lower degree of distorted CoO_{6-x} configuration would lead to a lower charge transfer resistance according to both EIS result in Figure 2c and in agreement with reported Co_3O_4 films.[23] When adding V to CoOOH, distortion of CoO_6 octahedron (CoO_{6-x}) occurs in $Co_{2-x}V_xO_4$ and the degree of the distortion depends on the vanadium amount introduced. Although CoO_{6-x} is beneficial for OER, too much distortion may also dramatically lead to excess oxygen vacancies, resulting in a significant reduction in the intrinsic OER activity as reported before.[15,23] Herein, the as-developed vanadium doping strategy not only adjusted the crystallinity of Co-V bimetallic oxides to the optimal CoO_{6-x} configuration but also led to the formation of Co^{3+}-O-V^{4+} active species under in-situ OER condition. The synergistic effect of the optimal CoO_{6-x} configuration and surface Co^{3+}-O-V^{4+} species resulted in a superior electrocatalyst for OER.

In summary, we discovered an efficient route to fabricate Co-V bimetallic oxides by controlling the molar ratio between cobalt and vanadium in the precursor solution. The component, crystallinity and morphology could be regulated by the Co/V ratio in the synthesis. It was found that the low-crystallinity $Co_{2-x}V_xO_4$ catalyst exhibited much higher activity than the amorphous or crystalline analogues due to the controlled distortion degree of CoO_6 apart from the very high concentration of Co^{3+} (Co^{3+}/Co^{2+} = 2.84). More importantly, it was demonstrated that the real

active species of Co^{3+}-O-V^{4+} could be in-situ derived from Co^{2+}-O-V^{5+} during the OER, forming low-crystallinity of $Co_{2-x}V_xO_4$ as observed by Operando XANES and in-situ XPS analysis. The optimised electrocatalyst displayed the smallest overpotential of 240 mV at 10 mA/cm2, excellent durability for OER in 1 M KOH and the Tafel slope of 45 mV dec^{-1}. The current density at η = 280 mV is 100 mA/cm2 for the optimised LC-$Co_{2-x}V_xO_4$, nearly 600 times higher than that of CoOOH. The overpotential is also nearly 130 mV lower than that of the widely reported CoOOH catalyst and also outperformed that of the commercial RuO_2. This will open up opportunities to advance the electrochemical performance of non-precious OER electrocatalysts by V^{4+} stabilised reaction center and precisely manipulating crystallinity.

ASSOCIATED CONTENT

Supporting Information

The supporting information is available free of charge at XXX

Movie of stability simulation of $Co_{2-x}V_xO_4$ (AVI)

Experimental section, Figure S1-S6 , Tables S1-S3, and supporting references (PDF)

AUTHOR INFORMATION

Corresponding Author

Junwang Tang - Department of Chemical Engineering, University College London, Torrington Place, London, WC1E 7JE, UK;

Email: junwang. tang @ucl.ac.uk

Aiqin Wang - State Key Laboratory of Catalysis, Dalian Institute of Chemical Physics, Chinese Academy of Sciences, Dalian, 116023, China;
Email: aqwang@dicp.ac.cn

Authors

Chaoran Jiang - Department of Chemical Engineering, University College London, Torrington Place, London, WC1E 7JE, UK

Ji Yang - State Key Laboratory of Catalysis, Dalian Institute of Chemical Physics, Chinese Academy of Sciences, Dalian, 116023, China; State Key Laboratory of Physical Chemistry of Solid Surfaces, iChEM, and College of Chemistry and Chemical Engineering, Xiamen University, Xiamen, 361005, P.R. China

Haifeng Qi - State Key Laboratory of Catalysis, Dalian Institute of Chemical Physics, Chinese Academy of Sciences, Dalian, 116023, P.R. China

Xiaoyu Han – Department of Chemistry, University of Manchester, Oxford Road, Manchester, M13 9PL, UK.

Min Su - State Key Laboratory of Physical Chemistry of Solid Surfaces, iChEM, and College of Chemistry and Chemical Engineering, Xiamen University, Xiamen, 361005, P.R. China

Deqiang Zhao - Department of Chemical Engineering, University College London, Torrington Place, London, WC1E 7JE, UK

Leilei Kang - State Key Laboratory of Catalysis, Dalian Institute of Chemical Physics, Chinese Academy of Sciences, Dalian, 116023, P.R. China

Xiaoyan Liu - State Key Laboratory of Catalysis, Dalian Institute of Chemical Physics, Chinese Academy of Sciences, Dalian, 116023, P.R. China

Jianfeng Ye - Department of Chemical Engineering, University College London, Torrington Place, London, WC1E 7JE, UK

Jian-Feng Li - State Key Laboratory of Physical Chemistry of Solid Surfaces, iChEM, and College of Chemistry and Chemical Engineering, Xiamen University, Xiamen, 361005, P.R.China

Zheng-Xiao Guo - Department of Chemistry, The university of Hong Kong, Pokfulam Road, Hongkong, 999077, P.R.China; HKU Zhejiang Institute of Research and Innovation, Hangzhou,311300,P.R.China.

Nikolas Kaltsoyannis – Department of Chemistry, University of Manchester, Oxford Road, Manchester, M13 9PL, UK

REFERENCES

(1) Yeo, B. S., Oxygen evolution by stabilized single Ru atoms. *Nat. Catal.* **2019**, 2 (4), 284-285.

(2) Li, P.; Wang, M.; Duan, X.; Zheng, L.; Cheng, X.; Zhang, Y.; Kuang, Y.; Li, Y.; Ma, Q.; Feng, Z.; Liu, W.; Sun, X., Boosting oxygen evolution of single-atomic ruthenium through electronic coupling with cobalt-iron layered double hydroxides. *Nat. Commun.* **2019**, 10 (1), 1711.

(3) Suen, N. T.; Hung, S. F.; Quan, Q.; Zhang, N.; Xu, Y. J.; Chen, H. M., Electrocatalysis for the oxygen evolution reaction: recent development and future perspectives. *Chem. Soc. Rev.* **2017**, 46 (2), 337-365.

(4) Jiang, C. R.; Wu, J.; Moniz, S. J. A.; Guo, D.; Tang, M.; Jiang, Q.; Chen, S.; Liu, H.; Wang, A. Q.; Zhang, T.; Tang, J. W., Stabilization of GaAs photoanodes by in-situ deposition of nickel-borate surface catalyst as hole trapping sites. *Sustain. Energy Fuels* **2019**, (3), 814-822.

(5) Frydendal, R.; Paoli, E. A.; Knudsen, B. P.; Wickman, B.; Malacrida, P.; Stephens, I. E. L.; Chorkendorff, I., Benchmarking the Stability of Oxygen Evolution Reaction Catalysts: The Importance of Monitoring Mass Losses. *ChemElectroChem* **2014**, 1 (12), 2075-2081.

(6) Lee, Y.; Suntivich, J.; May, K. J.; Perry, E. E.; Shao-Horn, Y., Synthesis and Activities of Rutile IrO_2 and RuO_2 Nanoparticles for Oxygen Evolution in Acid and Alkaline Solutions. *J. Phys. Chem. Lett.* **2012**, 3 (3), 399-404.

(7) Jiang, C.; Moniz, S. J.; Wang, A.; Zhang, T.; Tang, J., Photoelectrochemical devices for solar water splitting–materials and challenges. *Chem. Soc. Rev.* **2017**, (46), 4645-4660.

(8) Luo, W.; Jiang, C.; Li, Y.; Shevlin, S. A.; Han, X.; Qiu, K.; Cheng, Y.; Guo, Z.; Huang, W.; Tang, J., Highly crystallized [small alpha]-FeOOH for a stable and efficient oxygen evolution reaction. *J. Mater. Chem. A* **2017**, 5 (5), 2021-2028.

(9) Wang, J.; Cui, W.; Liu, Q.; Xing, Z.; Asiri, A. M.; Sun, X., Recent Progress in Cobalt-Based Heterogeneous Catalysts for Electrochemical Water Splitting. *Adv. Mater.* **2016**, 28 (2), 215-230.

(10) Grimaud, A.; May, K. J.; Carlton, C. E.; Lee, Y. L.; Risch, M.; Hong, W. T.; Zhou, J.; Shao-Horn, Y., Double perovskites as a family of highly active catalysts for oxygen evolution in alkaline solution. *Nat. Commun.* **2013**, 4, 2439.

(11) Wei, C.; Feng, Z.; Scherer, G. G.; Barber, J.; Shao-Horn, Y.; Xu, Z. J., Cations in Octahedral Sites: A Descriptor for Oxygen Electrocatalysis on Transition-Metal Spinels. *Adv. Mater.* **2017**, 29 (23), 1606800.

(12) Petrie, J. R.; Jeen, H.; Barron, S. C.; Meyer, T. L.; Lee, H. N., Enhancing Perovskite Electrocatalysis through Strain Tuning of the Oxygen Deficiency. *J. Am. Chem. Soc.* **2016**, 138 (23), 7252-7255.

(13) Maiyalagan, T.; Jarvis, K. A.; Therese, S.; Ferreira, P. J.; Manthiram, A., Spinel-type lithium cobalt oxide as a bifunctional electrocatalyst for the oxygen evolution and oxygen reduction reactions. *Nat. Commun.* **2014**, 5, 3949.

(14) Ye, S. H.; Shi, Z. X.; Feng, J. X.; Tong, Y. X.; Li, G. R., Activating CoOOH Porous Nanosheet Arrays by Partial Iron Substitution for Efficient Oxygen Evolution Reaction. *Angew. Chem., Int. Ed.* **2018**, 57 (10), 2672-2676.

(15) Xiao, Z.; Huang, Y. C.; Dong, C. L.; Xie, C.; Liu, Z.; Du, S.; Chen, W.; Yan, D.; Tao, L.; Shu, Z., Operando identification of the dynamic behavior of oxygen vacancy-rich Co_3O_4 for oxygen evolution reaction. *J. Am. Chem. Soc.* **2020**, 142 (28), 12087-12095.

(16) Li, S.; Peng, S.; Huang, L.; Cui, X.; Al-Enizi, A. M.; Zheng, G., Carbon-coated Co^{3+}-rich cobalt selenide derived from ZIF-67 for efficient electrochemical water oxidation. *ACS Appl. Mater. Interfaces* **2016**, 8 (32), 20534-20539.

(17) Liu, H.; Liu, X.; Mao, Z.; Zhao, Z.; Peng, X.; Luo, J.; Sun, X., Plasma-activated $Co_3(PO_4)_2$ nanosheet arrays with Co^{3+}-Rich surfaces for overall water splitting. *J. Power Sources* **2018**, (400), 190-197.

(18) Zhang, H.; Chen, B.; Jiang, H.; Duan, X.; Zhu, Y.; Li, C., Boosting water oxidation electrocatalysts with surface engineered amorphous cobalt hydroxide nanoflakes. *Nanoscale* **2018**, 10 (27), 12991-12996.

(19) Pramanik, M.; Li, C.; Imura, M.; Malgras, V.; Kang, Y.-M.; Yamauchi, Y., Ordered Mesoporous Cobalt Phosphate with Crystallized Walls toward Highly Active Water Oxidation Electrocatalysts. *Small* **2016**, 12 (13), 1709-1715.

(20) Xu, Z.; Yan, S. C.; Shi, Z.; Yao, Y. F.; Zhou, P.; Wang, H. Y.; Zou, Z. G., Adjusting the Crystallinity of Mesoporous Spinel $CoGa_2O_4$ for Efficient Water Oxidation. *ACS Appl. Mater. Interfaces* **2016**, 8 (20), 12887-12893.

(21) Bergmann, A.; Martinez-Moreno, E.; Teschner, D.; Chernev, P.; Gliech, M.; de Araújo, J. F.; Reier, T.; Dau, H.; Strasser, P., Reversible amorphization and the catalytically active state of crystalline Co_3O_4 during oxygen evolution. *Nat. Commun.* **2015**, 6, 8625.

(22) Hsu, S. H.; Hung, S. F.; Wang, H. Y.; Xiao, F. X.; Zhang, L.; Yang, H.; Chen, H. M.; Lee, J. M.; Liu, B., Tuning the Electronic Spin State of Catalysts by Strain Control for Highly Efficient Water Electrolysis. *Small Methods* **2018**, 2 (5), 1800001.

(23) Miao, X.; Wu, L.; Lin, Y.; Yuan, X.; Zhao, J.; Yan, W.; Zhou, S.; Shi, L., The role of oxygen vacancies in water oxidation for perovskite cobalt oxide electrocatalysts: are more better? *Chem. Comm.* **2019**, 55 (10), 1442-1445.

(24) Tong, Y.; Guo, Y.; Chen, P.; Liu, H.; Zhang, M.; Zhang, L.; Yan, W.; Chu, W.; Wu, C.; Xie, Y., Spin-State Regulation of Perovskite Cobaltite to Realize Enhanced Oxygen Evolution Activity. *Chem* **2017**, 3 (5), 812-821.

(25) Jin, Y. Z.; Li, Z.; Wang, J. Q.; Li, R.; Li, Z. Q.; Liu, H.; Mao, J.; Dong, C. K.; Yang, J.; Qiao, S. Z.; Du, X. W., Tuning Spin State of Rock-Salt-Based Oxides by Manipulation of Crystallinity for Efficient Oxygen Electrocatalysis. *Adv. Energy Mater.* **2018**, 8 (22), 1703469.

(26) Pauporté, T.; Mendoza, L.; Cassir, M.; Bernard, M.; Chivot, J., Direct low-temperature deposition of crystallized CoOOH films by potentiostatic electrolysis. *J. Electrochem. Soc.* **2005**, 152 (2), C49-C53.

(27) Liu, Y. C.; Koza, J. A.; Switzer, J. A., Conversion of electrodeposited $Co(OH)_2$ to CoOOH and Co_3O_4, and comparison of their catalytic activity for the oxygen evolution reaction. *Electrochim. Acta* **2014**, 140, 359-365.

(28) Chen, Z.; Kronawitter, C. X.; Yeh, Y. W.; Yang, X.; Zhao, P.; Yao, N.; Koel, B. E., Activity of pure and transition metal-modified CoOOH for the oxygen evolution reaction in an alkaline medium. *J Mater. Chem. A* **2017**, 5 (2), 842-850.

(29) Shi, H.; Liang, H.; Ming, F.; Wang, Z., Efficient Overall Water - Splitting Electrocatalysis Using Lepidocrocite VOOH Hollow Nanospheres. *Angew. Chem., Int. Ed.* **2017**, 129 (2), 588-592.

(30) Julien, C.; Nazri, G.; Bergström, O., Raman scattering studies of microcrystalline V_6O_{13}. *PSSBR* **1997**, 201 (1), 319-326.

(31) Chen, W.; Mai, L.; Peng, J.; Xu, Q.; Zhu, Q., Raman spectroscopic study of vanadium oxide nanotubes. *J. Solid State Chem.* **2004**, 177 (1), 377-379.

(32) Van Landschoot, N.; Kelder, E. M.; Schoonman, J., Citric acid-assisted synthesis and characterization of doped $LiCoVO_4$. *Solid State Ion.* **2004**, 166 (3), 307-316.

(33) Frost, R. L.; Henry, D. A.; Weier, M. L.; Martens, W., Raman spectroscopy of three polymorphs of $BiVO_4$: clinobisvanite, dreyerite and pucherite, with comparisons to $(VO_4)_3$ - bearing minerals: namibite, pottsite and schumacherite. *J. Raman Spectrosc.* **2006**, 37 (7), 722-732.

(34) Julien, C.; Massot, M.; Perez-Vicente, C., Structural and vibrational studies of $LiNi_{1-y}Co_yVO_4$ ($o \leqslant y \leqslant 1$) cathodes materials for Li-ion batteries. *Mater. Sci. Eng.: B* **2000**, 75 (1), 6-12.

(35) Jiang, C.; Yang, J.; Zhao, T.; Xiong, L.; Guo, Z.-X.; Ren, Y.; Qi, H.; Wang, A.; Tang, J., Co^{3+}-O-V^{4+} cluster in $CoVO_x$ nanorods for effi-

cient and stable electrochemical oxygen evolution. *Appl. Catal. B: Environ.* **282**, 119571.

(36) Chen, J.; Shi, W.; Yang, S.; Arandiyan, H.; Li, J., Distinguished Roles with Various Vanadium Loadings of CoCr$_{2-x}$V$_x$O$_4$ (x = 0–0.20) for Methane Combustion. J. Phys. Chem. C 2011, 115 (35), 17400-17408.

(37) Huang, Z. F.; Song, J.; Du, Y.; Xi, S.; Dou, S.; Nsanzimana, J. M. V.; Wang, C.; Xu, Z. J.; Wang, X., Chemical and structural origin of lattice oxygen oxidation in Co–Zn oxyhydroxide oxygen evolution electrocatalysts. *Nat. Energy* **2019**, 4 (4), 329-338.

(38) Zhang, B.; Zheng, X.; Voznyy, O.; Comin, R.; Bajdich, M.; García-Melchor, M.; Han, L.; Xu, J.; Liu, M.; Zheng, L.; García de Arquer, F. P.; Dinh, C. T.; Fan, F.; Yuan, M.; Yassitepe, E.; Chen, N.; Regier, T.; Liu, P.; Li, Y.; De Luna, P.; Janmohamed, A.; Xin, H. L.; Yang, H.; Vojvodic, A.; Sargent, E. H., Homogeneously dispersed multimetal oxygen-evolving catalysts. *Science* **2016**, 352 (6283), 333-337.

(39) Liardet, L.; Hu, X., Amorphous Cobalt Vanadium Oxide as a Highly Active Electrocatalyst for Oxygen Evolution. *ACS Catal.* **2018**, 8 (1), 644-650.

(40) Fan, K.; Chen, H.; Ji, Y.; Huang, H.; Claesson, P. M.; Daniel, Q.; Philippe, B.; Rensmo, H.; Li, F.; Luo, Y., Nickel-vanadium monolayer double hydroxide for efficient electrochemical water oxidation. *Nat. Commun.* **2016**, 7 (1), 11981.

(41) Fan, K.; Ji, Y.; Zou, H.; Zhang, J.; Zhu, B.; Chen, H.; Daniel, Q.; Luo, Y.; Yu, J.; Sun, L., Hollow Iron–Vanadium Composite Spheres: A Highly Efficient Iron-Based Water Oxidation Electrocatalyst without the Need for Nickel or Cobalt. Angew. Chem., Int. Ed. 2017, 56 (12), 3289-3293.

(42) Song, F.; Hu, X., Ultrathin Cobalt–Manganese Layered Double Hydroxide Is an Efficient Oxygen Evolution Catalyst. *J. Am. Chem. Soc.* **2014**, 136 (47), 16481-16484.

(43) Chang, C. J.; Chu, Y. C.; Yan, H. Y.; Liao, Y. F.; Chen, H. M., Revealing the structural transformation of rutile RuO$_2$ via in situ X-ray absorption spectroscopy during the oxygen evolution reaction. *Dalton Trans.* **2019**, (48), 7122-7129.

(44) Zhang, S.; Zhang, L.; Li, H.; Li, J.; Jiang, Z.; Chu, W.; Huang, Y.; Wang, J.; Wu, Z., Investigation of annealing-induced oxygen vacancies in the Co-doped ZnO system by Co K-edge XANES spectroscopy. *J. synchrotron radiat.* **2010**, 17 (5), 600-605.

(45) Liu, J.; Ji, Y.; Nai, J.; Niu, X.; Luo, Y.; Guo, L.; Yang, S., Ultrathin amorphous cobalt–vanadium hydr(oxy)oxide catalysts for the oxygen evolution reaction. *Energ. Environ. Sci.* **2018**, 11 (7), 1736-1741.

(46) Chakrapani, K.; Bendt, G.; Hajiyani, H.; Lunkenbein, T.; Greiner, M. T.; Masliuk, L.; Salamon, S.; Landers, J.; Schlögl, R.; Wende, H.; Pentcheva, R.; Schulz, S.; Behrens, M., The Role of Composition of Uniform and Highly Dispersed Cobalt Vanadium Iron Spinel Nanocrystals for Oxygen Electrocatalysis. *ACS Catal.* **2018**, 8 (2), 1259-1267.

(47) Bao, J.; Wang, Z.; Xie, J.; Xu, L.; Lei, F.; Guan, M.; Zhao, Y.; Huang, Y.; Li, H., A ternary cobalt–molybdenum–vanadium layered double hydroxide nanosheet array as an efficient bifunctional electrocatalyst for overall water splitting. *Chem. Comm.* **2019**, 55 (24), 3521-3524.

(48) Huang, J.; Chen, J.; Yao, T.; He, J.; Jiang, S.; Sun, Z.; Liu, Q.; Cheng, W.; Hu, F.; Jiang, Y., CoOOH nanosheets with high mass activity for water oxidation. *Angew. Chem., Int. Ed.* **2015**, 127 (30), 8846-8851.

(49) Yang, J.; Liu, H.; Martens, W. N.; Frost, R. L., Synthesis and Characterization of Cobalt Hydroxide, Cobalt Oxyhydroxide, and Cobalt Oxide Nanodiscs. *J. Phys. Chem. C* **2010**, 114 (1), 111-119.

(50) Wang, J.; Gao, R.; Zhou, D.; Chen, Z.; Wu, Z.; Schumacher, G.; Hu, Z.; Liu, X., Boosting the electrocatalytic activity of Co$_3$O$_4$ nanosheets for a Li-O$_2$ battery through modulating inner oxygen vacancy and exterior Co^{3+}/Co^{2+} ratio. *ACS Catal.* **2017**, 7 (10), 6533-6541.

(51) Yan, K.-L.; Qin, J.-F.; Lin, J.-H.; Dong, B.; Chi, J.-Q.; Liu, Z.-Z.; Dai, F.-N.; Chai, Y.-M.; Liu, C.-G., Probing the active sites of Co$_3$O$_4$ for the acidic oxygen evolution reaction by modulating the Co^{2+}/Co^{3+} ratio. *J Mater. Chem. A* **2018**, 6 (14), 5678-5686.

(52) Yang, H.; Long, Y.; Zhu, Y.; Zhao, Z.; Ma, P.; Jin, J.; Ma, J., Crystal lattice distortion in ultrathin Co(OH)$_2$ nanosheets inducing elongated Co–OOH bonds for highly efficient oxygen evolution reaction. *Green Chem.* **2017**, 19 (24), 5809-5817.

(53) Jain, A.; Ong, S. P.; Hautier, G.; Chen, W.; Richards, W. D.; Dacek, S.; Cholia, S.; Gunter, D.; Skinner, D.; Ceder, G., Commentary: The Materials Project: A materials genome approach to accelerating materials innovation. *APLmaterials.* **2013**, *1*(1),011002.

(54) Liu, X, Prewitt, C. T. High-temperature X-ray diffraction study of Co$_3$O$_4$: Transition from normal to disordered spinel. *Phys.Chem. Miner.* **1990**, 17(2), 168-172.

Table of Contents Graphic